

The red-sequence of 72 WINGS local galaxy clusters

T. Valentinuzzi¹, B.M. Poggianti², G. Fasano², M. D’Onofrio¹, A. Moretti², M. Ramella³, A. Biviano³, J. Fritz⁴, J. Varela², A. Cava⁵, D. Bettoni², B. Vulcani^{2,1}, M. Moles⁶, W.J. Couch⁷, A. Dressler⁸, and P. Kjærsgaard⁹ A. Omizzolo²

¹ Astronomy Department, University of Padova, Vicolo Osservatorio 2, 35122 Padova, Italy

² INAF – Padova Astronomical Observatory, Vicolo Osservatorio 5, 35122 Padova, Italy

³ INAF – Trieste Astronomical Observatory, via Tiepolo 11, 34131 Trieste, Italy

⁴ Sterrenkundig Observatorium Vakgroep Fysica en Sterrenkunde Univeriteit Gent, Gent, Belgium

⁵ Departamento de Astrofísica, Universidad Complutense de Madrid, Spain

⁶ Centro de Estudios de Física del Cosmos de Aragón, Plaza de San Juan 1, 44001 Teruel, Spain

⁷ Centre for Astrophysics & Supercomputing, Swinburne University, Hawthorn 3122, VIC, Australia

⁸ Observatories of the Carnegie Institution of Washington, Pasadena, CA 91101, USA

⁹ The Niels Bohr Institute, Juliane Maries Vej 30, 2100 Copenhagen, Denmark

November 12, 2018

ABSTRACT

We study the color-magnitude red sequence and blue fraction of 72 X-ray selected galaxy clusters at $z = 0.04 - 0.07$ from the WINGS survey, searching for correlations between the characteristics of the red sequence and the environment. We consider the slope and scatter of the red sequence, the number ratio of red luminous-to-faint galaxies, the blue fraction and the fractions of ellipticals, S0s and spirals that compose the red sequence. None of these quantities correlate with the cluster velocity dispersion, X-ray luminosity, number of cluster substructures, BCG prevalence over next brightest galaxies and spatial concentration of ellipticals. Instead, the properties of the red sequence depend strongly on local galaxy density. Higher density regions have a lower RS scatter, a higher luminous-to-faint ratio, a lower blue fraction, and a lower spiral fraction on the RS. Our results highlight the prominent effect of the local density in setting the epoch when galaxies become passive and join the red sequence, as opposed to the mass of the galaxy host structure.

Key words. Surveys – Galaxies : Clusters : General – Galaxies: evolution – Galaxies: star formation – Galaxies: structure

1. Introduction

The location of galaxies in a color-absolute magnitude diagram has traditionally been one of the chief methods to examine the stellar population properties of galaxies and their evolution.

The importance of the color-magnitude diagram in galaxy studies can hardly be overstated. Very early studies (de Vaucouleurs 1961; Visvanathan & Sandage 1977) recognized the existence in such a diagram of a “red sequence” (hereafter, RS), where early-type galaxies lie, also known as the “color-magnitude relation” (CMR) because it represents a positive correlation between galaxy color and luminosity.

The RS represents an easily recognizable feature in the color-magnitude diagram that can be used, to first approximation, to separate red, passively evolving galaxies devoid of star formation, from bluer star-forming galaxies.

Innumerable studies have investigated the origin of such a relation, and the reasons why a galaxy belongs to it, or falls below it at bluer colors.

The slope, scatter and location of the RS have long been used to place constraints on the formation epoch of stars in early-type galaxies (Bower et al. 1992; Ellis et al. 1997; Kodama et al. 1998). The RS is most conspicuous in galaxy clusters, that are rich in passive early-type galaxies. A well-defined RS has been observed in clusters up to high redshifts (Lidman et al. 2008; Mei et al. 2009; Strazzullo et al. 2010) and the fact that the galaxies with the oldest stars preferentially inhabit clusters at any epoch can be used to identify galaxy clusters, using their RS,

up to high redshifts (Gladders & Yee 2005; Muzzin et al. 2009; Wilson et al. 2009; Gilbank et al. 2011).

Observations of the relative fractions of galaxies on and below the RS have uncovered evolution in the star formation activity within clusters (Butcher & Oemler 1984; Ellingson et al. 2001; Loh et al. 2008) and, more recently, in the field (Bell et al. 2004; Faber et al. 2007; Bell et al. 2007). It has thus become clear that a large number of galaxies have stopped forming stars and have turned from blue to red at z below 1 in all environments, but in a way that depends on environment. It is also now well established that this progressive “passivization” process of galaxies proceeds in a downsizing fashion, with more massive and luminous galaxies reaching the RS at earlier epochs than lower-mass, fainter galaxies (Cowie et al. 1996). Large spectroscopic surveys have confirmed and placed on a very solid statistical ground earlier results on the correspondence between the bimodality in colors (red and blue) and other main galaxy characteristics such as morphological type (early and late) and galaxy stellar mass (Strateva et al. 2001; Kauffmann et al. 2003; Cheng et al. 2011).

One of the main outstanding questions remains the physical reason why galaxies stop forming stars and become red. Naturally, there can be multiple physical mechanisms responsible for the end of star formation. Their relative importance might vary with galaxy mass, galaxy location (environment), and redshift, among other things (Peng et al. 2010).

Two mechanisms in particular have been the subject of extensive theoretical investigation in the last years: AGN quench-

ing, and strangulation by which the hot gas reservoir is removed from galaxies upon merging with a larger halo (Croton et al. 2006; Bower et al. 2006; van den Bosch et al. 2008; Guo et al. 2011; McCarthy et al. 2010). Models however are currently unable to reproduce the observed trends, and generally overproduce the fraction of red galaxies (Font et al. 2008; Balogh et al. 2009; Kimm et al. 2009). In clusters, additional mechanisms are expected and observed to take place, such as ram pressure stripping (Gunn & Gott 1972) and harassment (Moore et al. 1998), though they may be much more efficient than originally thought even in lower mass systems than clusters (Bekki 2009).

The main issue is clearly to what extent the end of star formation is due to internal galaxy properties, and to what extent it is related to the global environment (for example the halo mass of the galaxy host structure) or the local environment. In this paper we investigate the relation between the RS properties of galaxies in clusters and the global and local environmental properties in the local Universe. We use a survey of 77 X-ray selected nearby galaxy clusters (the Wide-field Nearby Galaxy-cluster Survey, WINGS) to search for correlations between the RS characteristics and the galaxy environment, with the aim of shedding some light on the mechanisms that result in the population of passive red galaxies in clusters today. WINGS clusters span a wide range of cluster masses, and their galaxies are found in widely different local environmental densities, thus allowing a broad investigation using a homogeneous, high quality photometric dataset.

In the following, we describe the WINGS dataset (§2) and the method used to define the RS (§3). In §4 we investigate if the RS characteristics (slope, scatter and value of the best fit line at $M_V = -20$), the ratio of the number of luminous to faint galaxies on the RS, the blue galaxy fraction and the morphological fractions of galaxies on the RS depend on general cluster properties (cluster velocity dispersion, X-ray luminosity, BCG dominance, number of substructures and concentration of ellipticals). We then study the same characteristics of the RS as a function of local galaxy density (§4.5). Our conclusions are summarized in §5.

Throughout this paper we use the cosmological parameters $(H_0, \Omega_m, \Omega_\Lambda) = (70 \text{ km s}^{-1} \text{ Mpc}^{-1}, 0.3, 0.7)$.

2. The Data

The galaxies examined in this paper are part of the *Wide-field Nearby Galaxy-clusters Survey* (Fasano et al. 2006). WINGS¹ is a multiwavelength survey designed to provide a robust characterization of the photometric and spectroscopic properties of galaxies in nearby clusters, and to determine the variations of these properties as a function of galaxy mass and environment.

Clusters were selected in the X-ray from the ROSAT Brightest Cluster Sample and its extension (Ebeling et al. 1998, 2000) and the X-ray Brightest Abell-type Cluster sample (Ebeling et al. 1996). WINGS clusters cover a wide range of velocity dispersion σ_{clus} , typically between 500 and 1100 km s^{-1} , and X-ray luminosity L_X , typically $0.2 - 5 \times 10^{44} \text{ erg/s}$.

The survey core dataset, consisting of optical B and V imaging of 78 nearby ($0.04 < z < 0.07$) galaxy-clusters (Varela et al. 2009), has been complemented by several ancillary projects: (i) a spectroscopic follow up of about 6500 galaxies in a subsample of 48 clusters, obtained with the spectrographs WYFFOS@WHT and 2dF@AAT (Cava et al. 2009);

(ii) near-infrared (J, K) imaging of a subsample of 28 clusters obtained with WFCAM@UKIRT (Valentinuzzi et al. 2009); (iii) U broad- and H_α narrow-band imaging of subsamples of WINGS clusters, obtained with wide-field cameras at different telescopes (INT, LBT, Bok, see Omizzolo et al. 2011, in preparation).

The B and V photometric catalogs used in this paper are described in detail in (Varela et al. 2009). Briefly, our catalogs are 90% complete at $V \sim 21.7$, and the star-galaxy separation was visually checked, making the number of misclassifications negligible, down to $V = 22$. The distance moduli of our clusters are in the range 36.1-37.4, therefore our photometric catalogs are highly complete and reliable down to $M_V = -15.7$ or fainter. The photometry was performed on images in which large galaxies and halos of bright stars were removed after modeling them with elliptical isophotes. This procedure greatly improved the photometry of the large galaxies and increased by 16% the detection rate of objects projected onto them (Varela et al. 2009).

WINGS galaxy morphologies were derived from V images using the purposely devised tool MORPHOT (Fasano et al., 2011 submitted, and Appendix A in Fasano et al. 2010). Our approach is a generalization of the non-parametric method proposed by Conselice et al. (2000) (see also, Conselice 2003). In particular, we have extended the classical CAS (Concentration/Asymmetry/clumpiness) parameter set by introducing a number of additional, suitably devised morphological indicators, using a final set of 11 parameters. A control sample of 1,000 visually classified galaxies has been used to calibrate the whole set of morphological indicators, with the aim of identifying the best sub-set among them, as well as of analyzing how they depend on galaxy size, flattening and S/N ratio. The morphological indicators have been combined with two independent methods, a Maximum Likelihood analysis and a Neural Network trained on the control sample of visually classified galaxies. The final, automatic morphological classification combines the results of both methods. We have verified that our automatic morphological classification reproduces well the visual classification by two of us (AD and GF). In particular, the robustness and reliability of the MORPHOT results turn out to be comparable with the typical values obtained comparing the visual classifications obtained by different experienced human classifiers (Fasano et al. 2011, in preparation).

All the following analysis is carried out for galaxies within $R_{200}/2$, where R_{200} (usually considered an approximation for the cluster virial radius) is the radius enclosing the sphere with interior mean density 200 times the critical density of the Universe at that redshift. The $R_{200}/2$ values were measured from the cluster velocity dispersions given in Table 1 as

$$R_{200} = 1.73 \frac{\sigma}{1000 \text{ km s}^{-1}} \frac{1}{\sqrt{\Omega_\Lambda + \Omega_0(1+z)^3}} h^{-1} \text{ Mpc} \quad (1)$$

After careful visual inspection of all the B-V versus V color-magnitude diagrams (CMDs) of our clusters, we decided to include only 72 clusters in this work because of incomplete radial coverage out to $R_{200}/2$ or nearly absent red sequence (RS).

In Table.1, we present a number of global properties of our clusters. Cluster redshifts are from Cava et al. (2009). Cluster velocity dispersions were derived, following the recipes given in Cava et al. (2009), from the WINGS database that collects, together with our data, all the available redshifts from NED. X-ray total luminosities are taken from Ebeling et al. (1996, 1998, 2000), and they have been converted to our adopted cosmology. The number of substructures found in each cluster are drawn

¹ Please refer to WINGS Website for updated details on the survey and its products, <http://web.oapd.inaf.it/wings>

from the analysis of Ramella et al. (2007), who searched for sub-structures in the projected distribution of galaxies in WINGS images using an adaptive-kernel procedure. The BCG prevalence value is determined with the following equation:

$$\text{BCG}_{\text{prev}} = (V_{\text{rank}2} + V_{\text{rank}3})/2 - V_{\text{rank}1} \quad (2)$$

where the V magnitudes refer to the first (the BCG), second and third ranked galaxies of the cluster. The higher the BCG prevalence value, the greater is the separation in magnitudes between the BCG and the next brightest cluster galaxies. It is believed that a system of galaxies, where most of the mass has been assembled very early, develops a larger magnitude gap between the brightest and second brightest galaxies compared to systems that form later (Dariush et al. 2010 and references therein), therefore the BCG_{prev} value would be somehow related to the main cluster “assembly epoch”. The concentration of elliptical galaxies (EsConc) is measured through a modified version of the Gini coefficient (Abraham et al. 2003; Lotz et al. 2004). In particular, we define this coefficient as the difference between the area subtended by the cumulative distribution function of the elliptical galaxies (rank-ordered according to their cluster-centric distance) and the diagonal of the square (Lorentz curve; for a perceptual illustration see figures 1 in Abraham et al. 2003; Lotz et al. 2004). In this formulation, the Gini coefficient increases as the concentration of galaxies toward the cluster center increases.

Finally, we measured galaxy local densities for each galaxy in our sample using the circular area (A_{10}) containing the 10 nearest projected neighbors in the photometric catalog (with or without spectroscopic membership) whose V -band absolute magnitude would be ≤ -19.5 if they were cluster members. As we only want to count as neighbours the members of the cluster, a statistical field correction has been applied to the counts using Table 5 in Berta et al. (2006). In particular, since the field counts in the area containing the 10 nearest neighbors are not integer numbers, A_{10} is obtained interpolating the two A_n areas for which the corrected counts (or the number of spectroscopic members, if greater than them) are immediately lower and greater than 10. A similar interpolation technique has also been used when the circular area containing the 10 nearest neighbors is not fully covered by the available data (galaxies at the edges of the WINGS field). In this case, at increasing n (and the corresponding area A_n), a coverage factor has been evaluated as the ratio between the circular area and the area actually covered by the observations. Then, the counts n have been scaled upwards to account for the corresponding coverage factors and then have been corrected for the field counts. Finally, as in the previous case, A_{10} has been obtained by interpolating the two A_n areas for which the corrected counts are immediately lower and greater than 10.

3. Red Sequence and Field Subtraction

One of the main issues in defining the red sequence of our clusters is the removal of the interloper galaxies. For all galaxies with redshift information, either from WINGS spectra or literature data, the cluster membership is known (Cava et al. 2009). In the absence of spectroscopy, the only alternative way is a statistical approach.

3.1. The interloper issue

The Monte Carlo statistical field subtraction technique is the standard method used (see *e.g.* Kodama & Bower 2001;

Pimbblet et al. 2002). We used the Berta et al. (2006) catalog of field galaxies in the ELAIS-S1 area (hereafter simply called FIELD), a cluster-free portion of the sky, to determine the number of contaminating galaxies as a function of magnitude and color. Both the WINGS (which comprehend cluster+field galaxies) and the FIELD data have been conveniently binned onto a grid in the color-magnitude diagram space. Obviously, for each cluster, the numbers of field galaxies in the grid are rescaled to the size of the field covered by WINGS.

Following Pimbblet et al. (2002), we defined the probability for each galaxy to be an interloper as follows:

$$P_{\text{int}}(\text{col}, \text{mag}) \equiv \frac{N_{\text{F}}(\text{col}, \text{mag})}{N_{\text{W}}(\text{col}, \text{mag})} \quad (3)$$

where N_{F} and N_{W} are the number of FIELD and WINGS galaxies in each (col, mag) bin, respectively. We further expanded the method to include all the redshift information we have: spectroscopically confirmed members N_{YES} and non-members N_{NO} were always retained and rejected, respectively, in the analysis.

Eq.(3) was modified accordingly:

$$P_{\text{int}} \equiv \frac{N_{\text{F}}(\text{col}, \text{mag}) - N_{\text{NO}}(\text{col}, \text{mag})}{N_{\text{W}}(\text{col}, \text{mag}) - N_{\text{NO}}(\text{col}, \text{mag}) - N_{\text{YES}}(\text{col}, \text{mag})} \quad (4)$$

One of the main caveats of this method is the possibility that the probability becomes negative: in this case we used the same recipe of Pimbblet et al. (2002), by applying an adaptive grid technique (for further details see Pimbblet et al. 2002, Appendix A). Once the interloper probability was determined at each grid position, we performed 100 Monte Carlo simulations generating a number between 0.0 and 1.0 for each galaxy. If the random number was greater than the corresponding P_{int} , than the galaxy was flagged as a member, otherwise it was assigned to the interloper population.

With this procedure the assumption that the FIELD sample is a *perfect* realization of the *real* interloper population is mitigated. Indeed, it can be demonstrated that with this procedure we are actually giving to each bin of the FIELD with N galaxies, a corresponding poissonian error of \sqrt{N} ; thus, it is like extracting at each run a new FIELD sample (a sort of bootstrap).

In Fig.1 we show the 37-th run of a Monte Carlo realization of the cluster Abell 119. In the upper panel all galaxies from the catalog are presented, but shown as green circles and blue crosses are the spectroscopic members and non-members, respectively. The use of the spectroscopic membership information is the only difference from the interloper subtraction used in Pimbblet et al. (2002). Red open circles and black filled dots refer to the galaxies assigned to the non-member and member population by the simulation. We also show the different morphologies, when available (see legend in the figure), of all cluster members (central panel) and only RS galaxies, as defined in the next section (bottom panel). Note the non-negligible presence of red spirals (blue and cyan open circles).

3.2. Defining the red sequence

We calculate rest frame absolute magnitudes and colors by applying a galaxy-type dependent k-correction based on the observed (B-V) color of the galaxies within an aperture (diameter) of 10.8kpc using the K-corrections from (Poggianti 1997). The physical aperture assures a well-sampled, distance-independent color for all galaxies. We further apply a cut in color $0.5 \leq (B - V)_{10.8\text{kpc}} \leq 1.5$ to eliminate those eventual (few) galaxies that are surely either too red or too blue to belong to our clusters

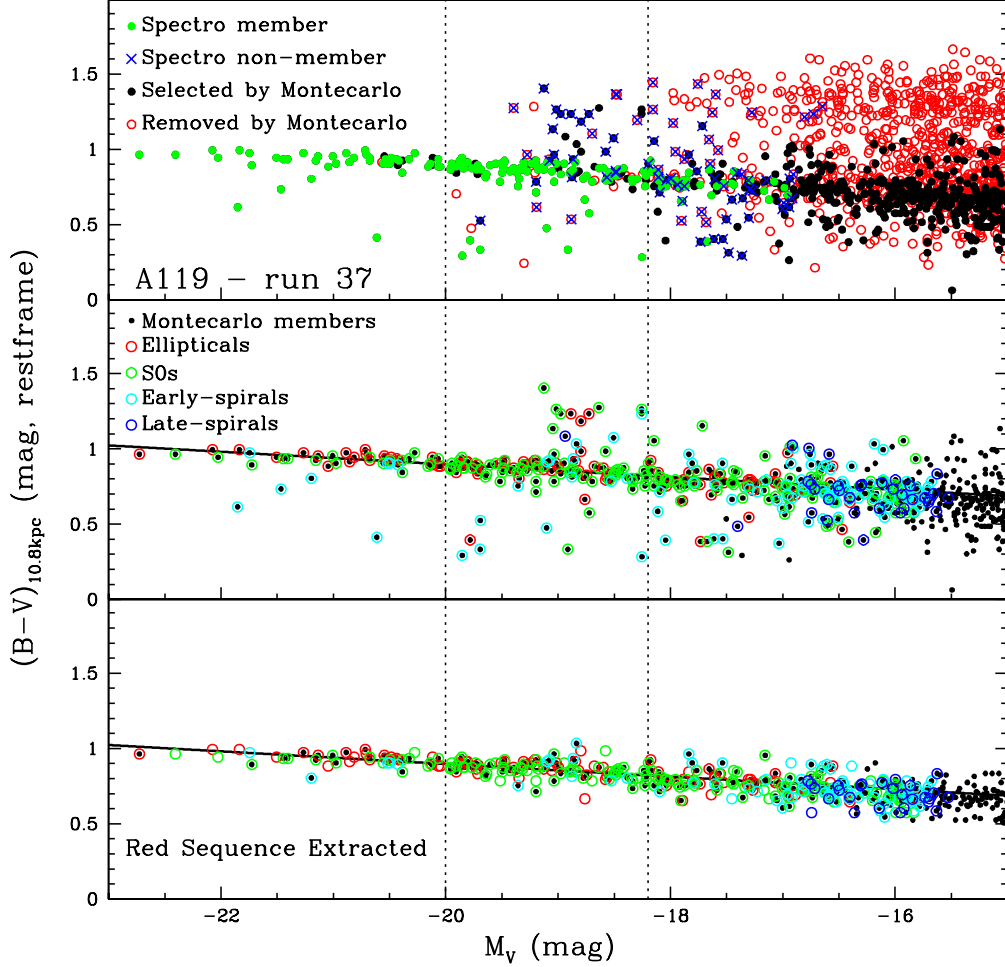


Fig. 1. Visual example of a Monte Carlo realization for the cluster Abell 119. In the upper panel, the red empty dots and the black filled dots are the non-members and members assigned by the simulation (run 37th), respectively. Shown as green circles and blue crosses are the spectroscopic members and non-members, respectively. In the middle panel only members according to the Montecarlo realization are shown, but divided in different morphological types (see legend and the figure in electronic format). In the bottom panel, the RS extracted is shown, again with the morphological color coding. The dotted vertical lines mark the absolute V magnitude limits used to define the Luminous and Faint population on the RS.

but might have remained after the statistical subtraction. In the following, we consider only galaxies brighter than $M_V \sim -18$ for which both our photometric and morphological catalogs are complete (Varela et al. 2009, Fasano et al. 2011).

We use the robust bi-weight estimator fitting procedure in two steps to identify the RS. The *first step* consists of fitting all the galaxies from the previous selection process with absolute V magnitude $-21.5 \leq M_V \leq -18$ and calculating the median distance d_{red} of all the galaxies from the best fit. We choose this magnitude interval because most of our CMDs (see Fig.1) exhibit a change of slope (are shallower) at higher luminosities,

of the second fit are assigned to the RS-population.² All non RS-galaxies bluer than that are assigned to the blue-population.

This procedure is applied to each of the 100 Montecarlo Simulations and a final mean value and its error are found for each individual cluster (see Table1). In Fig.(2) we present a sample plot of one of the Montecarlo realizations for each cluster, with the best fit parameters and the global scatter for the red sequence and the main properties of the cluster shown at the bottom of each panel. The vertical lines indicate the V-band absolute magnitude limits used to define the “Luminous” and the “Faint” red sequence population (see section 4.2).

In the *second step* only galaxies with $-21.5 \leq M_V \leq -18$ and distance $3 \times d_{red}$ from the previous step are fitted, and the RMS of the residuals is calculated. Only galaxies within 0.2 magnitudes

² Using galaxies within $2 \times \text{RMS}$ from the fit did not change any of the results of this paper.

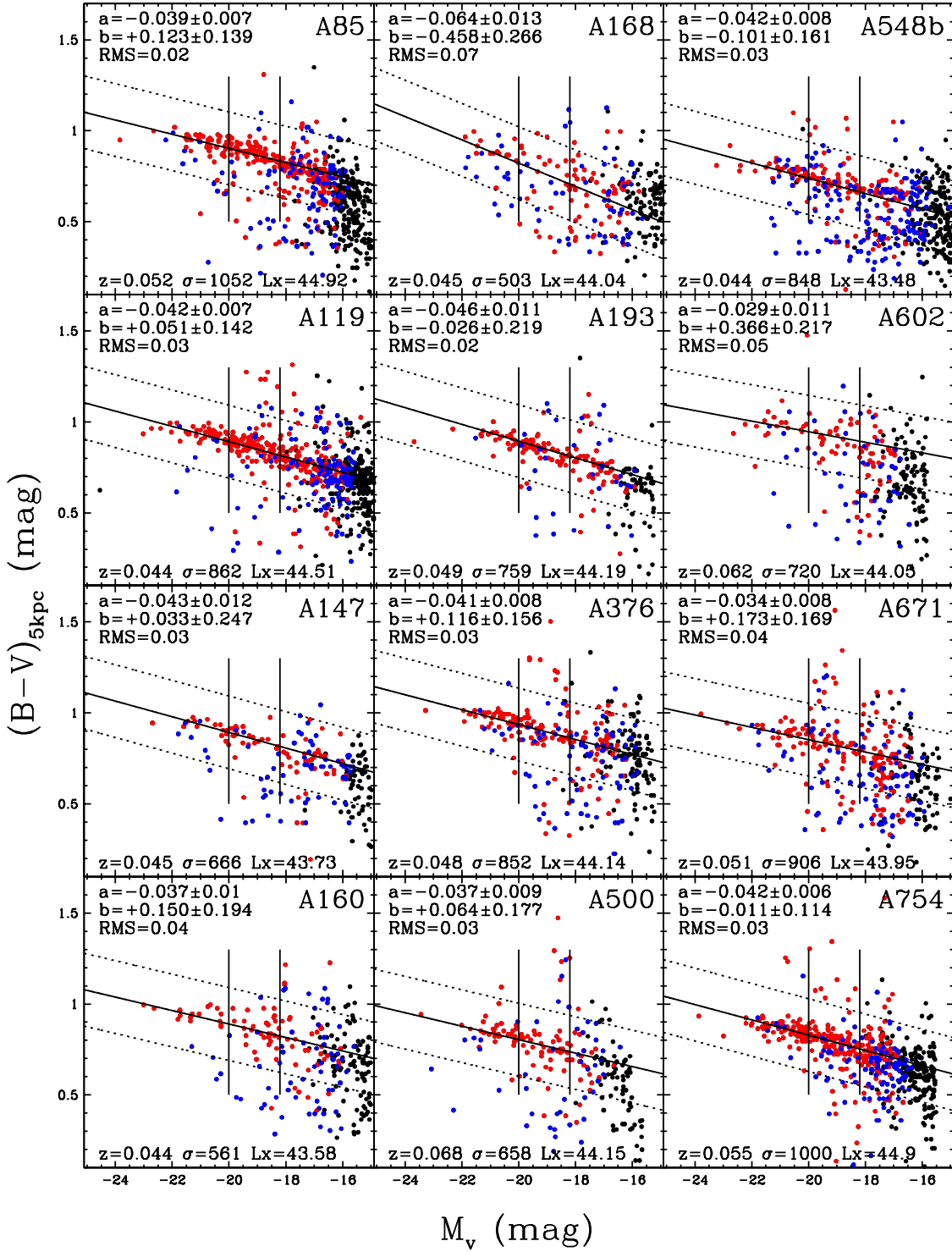


Fig. 2. A random realization of the Montecarlo interloper subtraction technique. Only galaxies assigned to the clusters are shown: red dots are morphologically early-type galaxies (Es and S0s), blue dots are late-type ones and black dots are galaxies with no available morphological classification (colors only available in the on-line version). The best fitted RS of the 100 realizations is drawn (solid black line) with ± 0.2 mag limits (dashed black lines) identifying the red sequence. The RMS numerical values are reported at the top of each panel. The global properties of each cluster are reported, for reference, at the bottom of each panel. The vertical lines mark the absolute V magnitude limits used to define the Luminous and the Faint population of the RS.

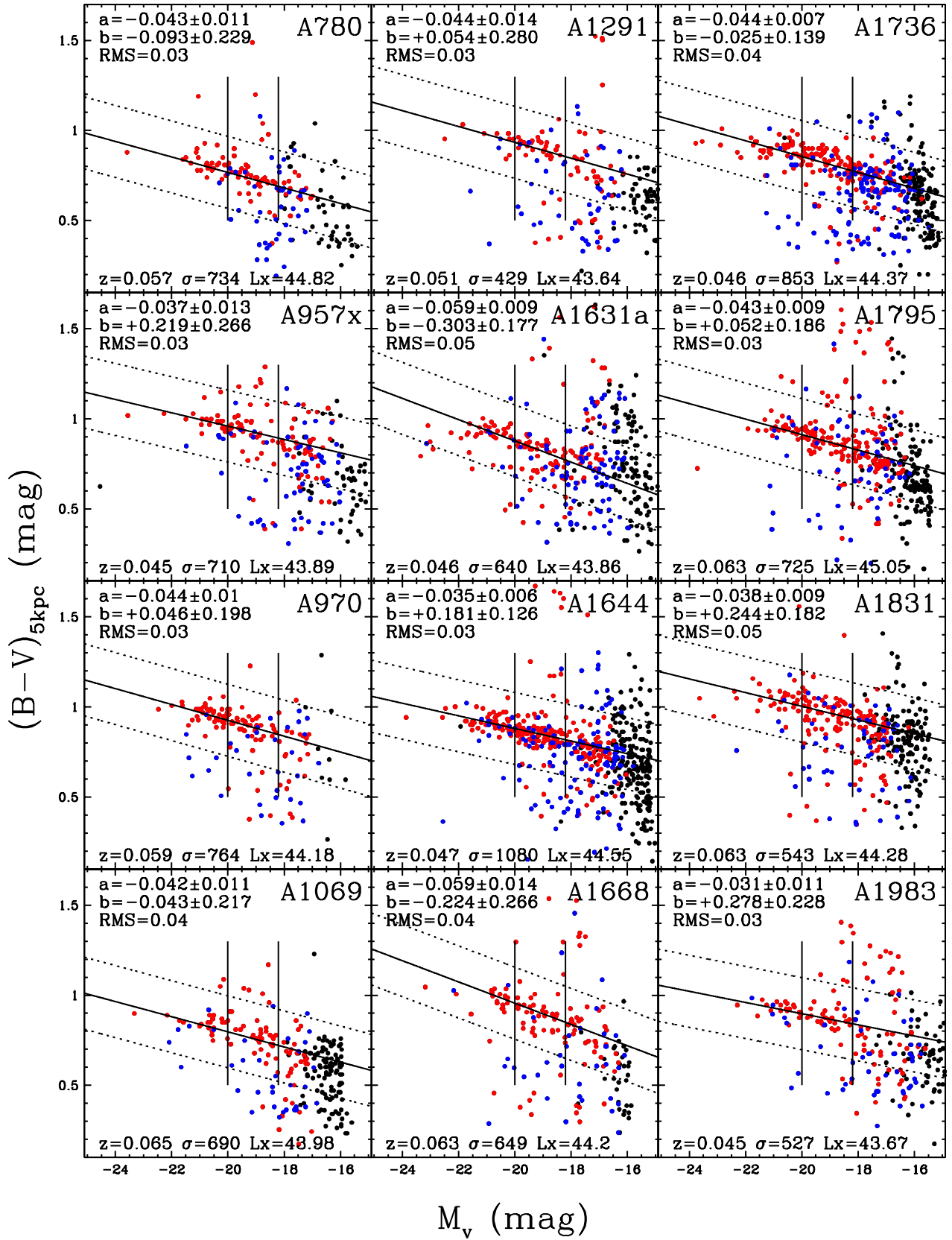


Fig. 2. continued.

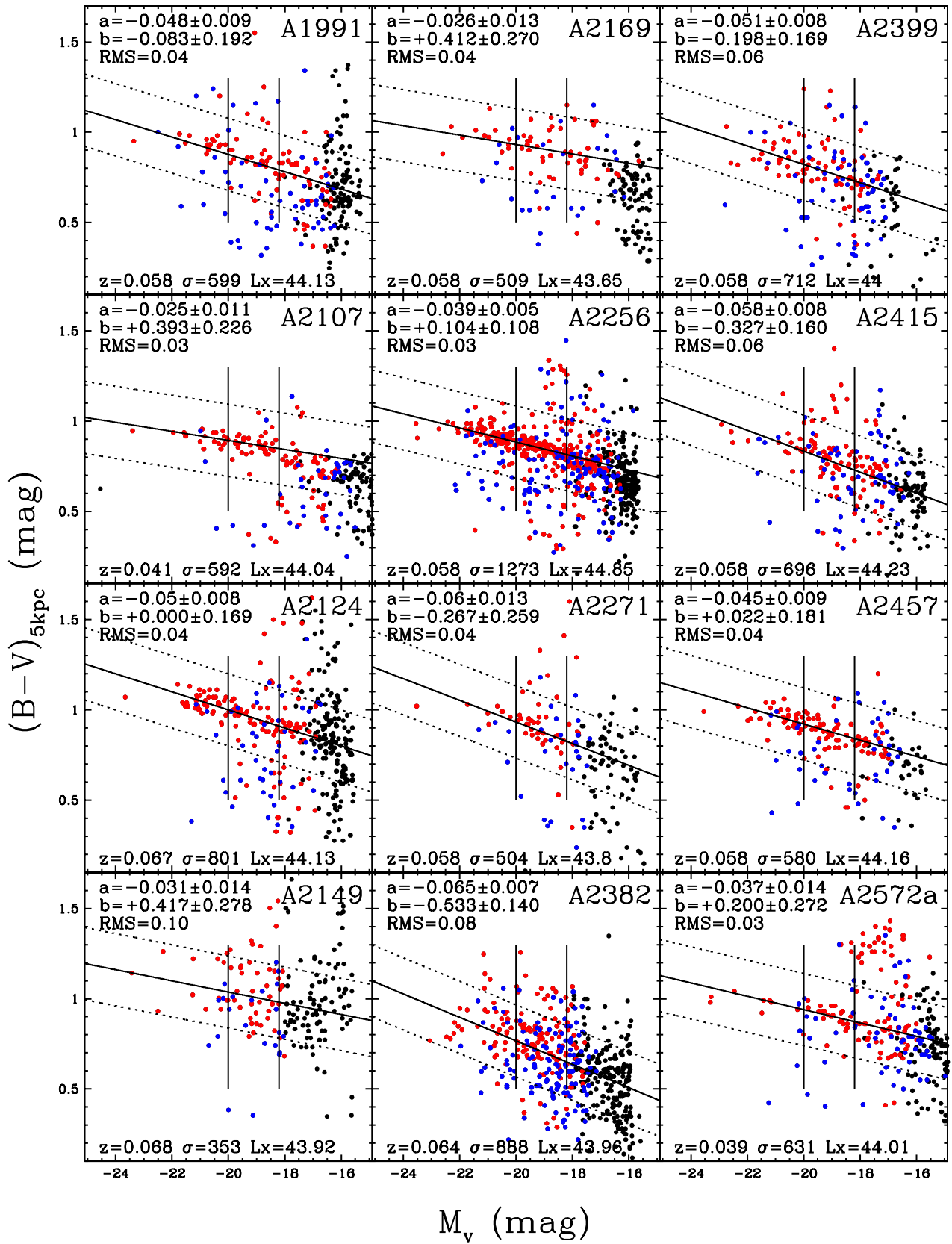


Fig. 2. continued.

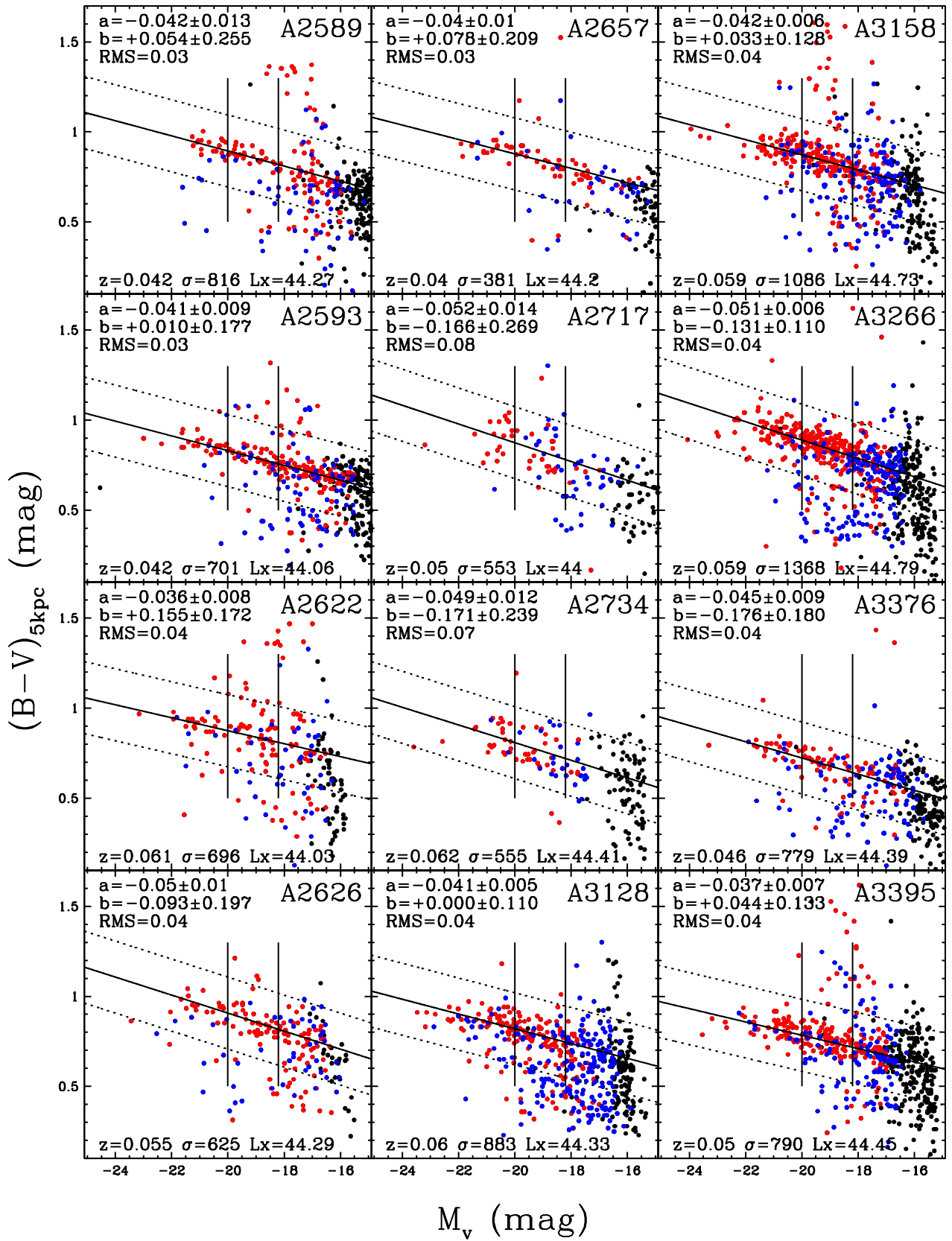


Fig. 2. continued.

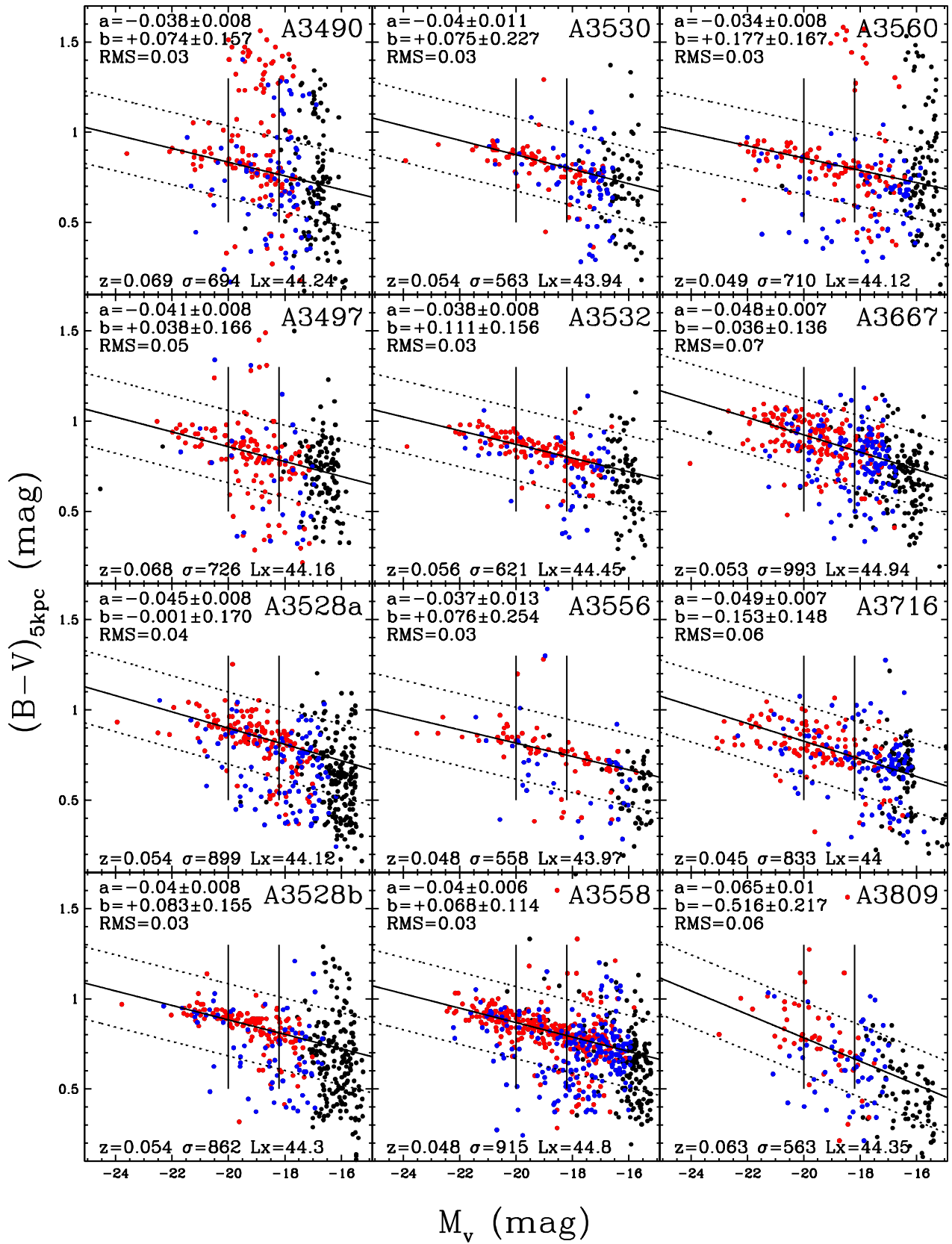


Fig. 2. continued.

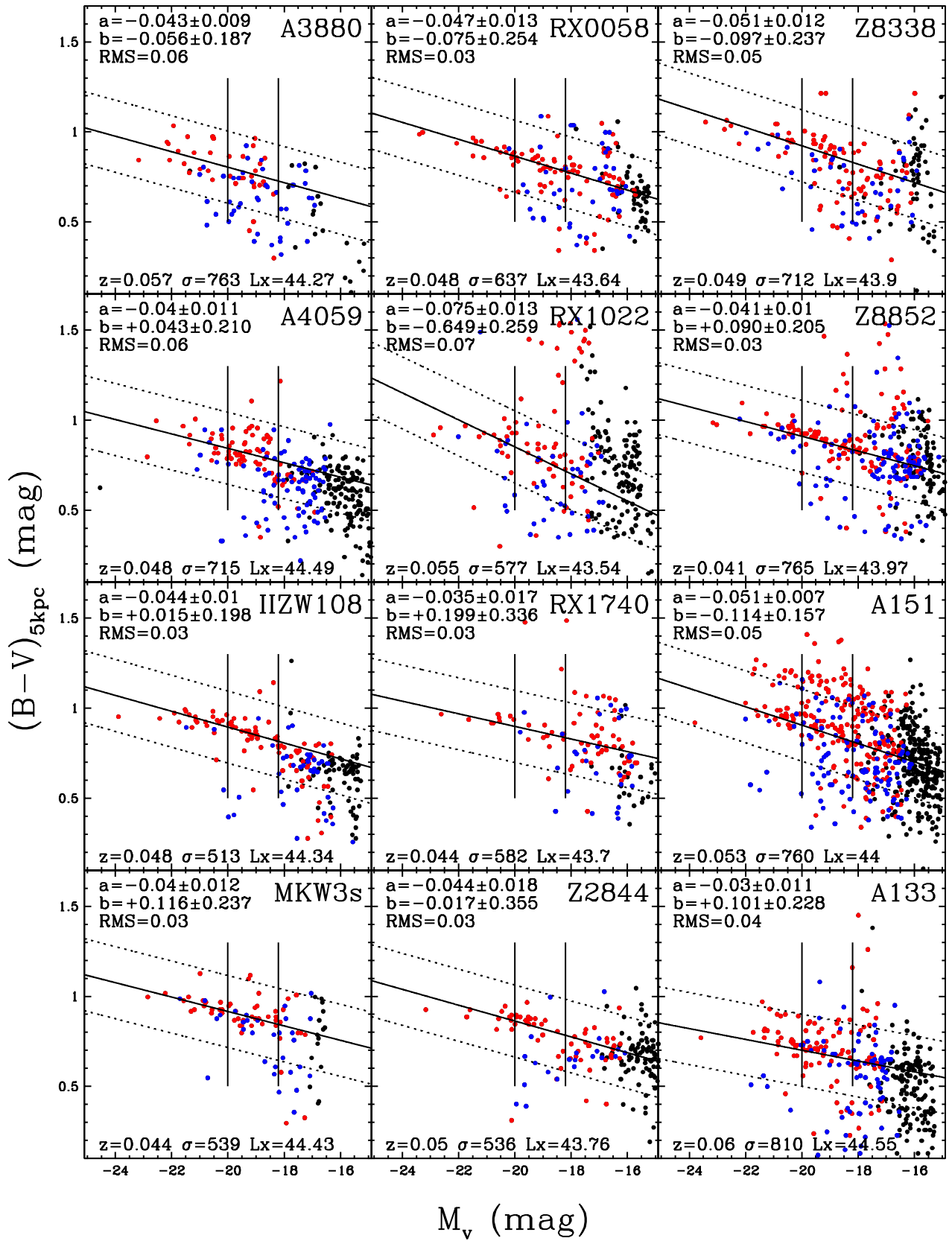


Fig. 2. End of Figure 2.

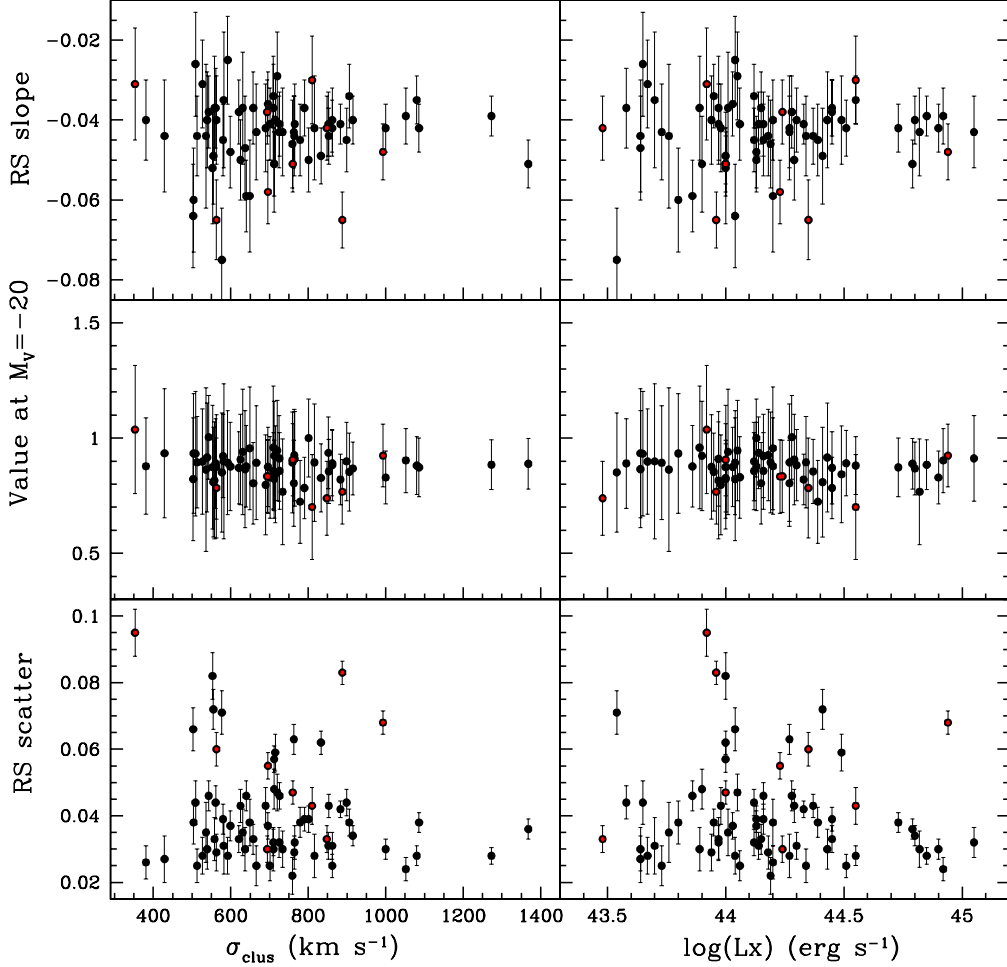


Fig. 3. Slope, value of best fit line at $M_V = -20$ and scatter of the median RS values of the 100 Montecarlo runs for each cluster versus cluster velocity dispersion (σ_{clus} , left panels) and cluster X-ray luminosity (L_X , right panels). Error bars refer to the error of the median of the 100 simulations. In red (on-line version), clusters whose RS is contaminated by another structure (see text).

4. Results

4.1. Slope and scatter

In Table 1, in addition to the global parameters of our cluster sample, we present the median slope and scatter of the 100 Monte Carlo realizations described in section 3.2. The median slope for all our clusters is -0.047 ± 0.001 , and the typical scatter is of the order of ~ 0.05 mag.

In Fig. 3 we plot the slope, the fit value at $M_V = -20$ and the scatter of the RS against the cluster velocity dispersion and total X-ray luminosity (both of which are related to the cluster mass). We have coloured in red those clusters whose RS appears to be contaminated by another galaxy structure visible in Fig. 2 (A133, A151, A548b, A2149, A2382, A2415, A3490, A3667, A3809),³ although it should be kept in mind that several other clusters have a very broad RS suggestive of more than one structure along the line of sight and close in redshift to the main cluster.

³ We have not highlighted here those clusters with a second RS that lies at sufficiently higher redshift not to be expected to influence the RS of the main WINGS structure, such as A2572, A3560, A3490, RX1022.

If the epoch and rate at which galaxies turn red and reach the color-magnitude RS depended upon the mass of the cluster to which galaxies belong at $z = 0$, we should observe a correlation between cluster mass and RS properties. Instead, we do not find any such correlation in our sample of 72 local clusters.

Similarly, we do not find any dependence of the RS slope, scatter, and $M_V = -20$ value on the number of substructures, the BCG prevalence value and the concentration of ellipticals (not shown). Our results agree with the previous findings of Stott et al. (2009) which showed a lack of correlation between the RS slope and the cluster σ , L_X and BCG dominance at $z = 0.1 - 1$.

4.2. Luminous-to-faint ratio and blue fractions

The number ratio of luminous-to-faint RS galaxies is often used to investigate the evolution of the faint end of the red luminosity function of cluster galaxies. High- z studies find a deficiency of faint red galaxies in comparison to local galaxy clusters, as the luminous-to-faint ratio is seen to evolve from higher values at high- z to lower values at low- z (see, among others, De Lucia et al. (2004); Tanaka et al. (2005); De Lucia et al.

Table 1.

Cluster	z	σ_{clus}	log(Lx)	Nsub	BCGprev	EsConc	slope	RMS
A85	0.052	1052.0	44.92	2	1.405	0.236	-0.039 ± 0.007	0.024
A119	0.044	862.0	44.51	2	0.990	0.179	-0.042 ± 0.007	0.025
A133	0.060	810.0	44.55	–	0.575	0.067	-0.030 ± 0.011	0.043
A147	0.045	666.0	43.73	2	0.505	0.162	-0.043 ± 0.012	0.025
A151	0.053	760.0	44.00	2	1.220	0.108	-0.051 ± 0.007	0.047
A160	0.044	561.0	43.58	3	0.485	0.119	-0.037 ± 0.010	0.044
A168	0.045	503.0	44.04	1	1.130	0.128	-0.064 ± 0.013	0.066
A193	0.049	759.0	44.19	0	1.000	0.164	-0.046 ± 0.011	0.022
A376	0.048	852.0	44.14	1	1.345	0.165	-0.041 ± 0.008	0.031
A500	0.068	658.0	44.15	1	0.435	0.175	-0.037 ± 0.009	0.033
A548b	0.044	848.0	43.48	–	0.635	0.127	-0.042 ± 0.008	0.033
A602	0.062	720.0	44.05	1	0.595	0.118	-0.029 ± 0.011	0.047
A671	0.051	906.0	43.95	2	1.070	0.207	-0.034 ± 0.008	0.038
A754	0.055	1000.0	44.90	2	1.140	0.164	-0.042 ± 0.006	0.030
A780	0.057	734.0	44.82	–	1.220	0.111	-0.043 ± 0.011	0.030
A957x	0.045	710.0	43.89	0	1.680	0.160	-0.037 ± 0.013	0.030
A970	0.059	764.0	44.18	1	0.290	0.214	-0.044 ± 0.010	0.029
A1069	0.065	690.0	43.98	1	1.030	0.186	-0.042 ± 0.011	0.043
A1291	0.051	429.0	43.64	1	0.785	0.144	-0.044 ± 0.014	0.027
A1631a	0.046	640.0	43.86	0	1.385	0.098	-0.059 ± 0.009	0.046
A1644	0.047	1080.0	44.55	–	1.275	0.000	-0.035 ± 0.006	0.028
A1668	0.063	649.0	44.20	–	1.060	0.153	-0.059 ± 0.014	0.038
A1736	0.046	853.0	44.37	5	0.145	0.177	-0.044 ± 0.007	0.043
A1795	0.063	725.0	45.05	1	1.480	0.185	-0.043 ± 0.009	0.032
A1831	0.063	543.0	44.28	1	0.875	0.067	-0.038 ± 0.009	0.046
A1983	0.045	527.0	43.67	–	0.275	0.126	-0.031 ± 0.011	0.028
A1991	0.058	599.0	44.13	1	0.855	0.102	-0.048 ± 0.009	0.037
A2107	0.041	592.0	44.04	0	1.395	0.080	-0.025 ± 0.011	0.028
A2124	0.067	801.0	44.13	0	1.945	0.124	-0.050 ± 0.008	0.039
A2149	0.068	353.0	43.92	0	0.945	0.128	-0.031 ± 0.014	0.095
A2169	0.058	509.0	43.65	0	0.315	0.011	-0.026 ± 0.013	0.044
A2256	0.058	1273.0	44.85	0	0.430	0.141	-0.039 ± 0.005	0.028
A2271	0.058	504.0	43.80	–	1.260	0.102	-0.060 ± 0.013	0.038
A2382	0.064	888.0	43.96	–	0.295	0.124	-0.065 ± 0.007	0.083
A2399	0.058	712.0	44.00	0	0.125	0.202	-0.051 ± 0.008	0.057
A2415	0.058	696.0	44.23	1	0.380	0.159	-0.058 ± 0.008	0.055
A2457	0.058	580.0	44.16	1	1.230	0.116	-0.045 ± 0.009	0.039
A2572a	0.039	631.0	44.01	3	0.440	0.094	-0.037 ± 0.014	0.035
A2589	0.042	816.0	44.27	–	2.030	0.104	-0.042 ± 0.013	0.028
A2593	0.042	701.0	44.06	1	0.995	0.212	-0.041 ± 0.009	0.025
A2622	0.061	696.0	44.03	1	1.220	0.128	-0.036 ± 0.008	0.037
A2626	0.055	625.0	44.29	–	1.120	0.142	-0.050 ± 0.010	0.043
A2657	0.040	381.0	44.20	1	0.865	0.008	-0.040 ± 0.010	0.026
A2717	0.050	553.0	44.00	–	1.030	0.129	-0.052 ± 0.014	0.082
A2734	0.062	555.0	44.41	3	0.860	0.149	-0.049 ± 0.012	0.072
A3128	0.060	883.0	44.33	3	0.315	0.114	-0.041 ± 0.005	0.042
A3158	0.059	1086.0	44.73	1	0.495	0.217	-0.042 ± 0.006	0.038
A3266	0.059	1368.0	44.79	0	1.065	0.235	-0.051 ± 0.006	0.036
A3376	0.046	779.0	44.39	2	0.870	0.089	-0.045 ± 0.009	0.038
A3395	0.050	790.0	44.45	–	0.575	0.138	-0.037 ± 0.007	0.039
A3490	0.069	694.0	44.24	–	0.375	0.111	-0.038 ± 0.008	0.030
A3497	0.068	726.0	44.16	–	0.340	0.076	-0.041 ± 0.008	0.046
A3528a	0.054	899.0	44.12	–	1.470	0.135	-0.045 ± 0.008	0.044
A3528b	0.054	862.0	44.30	1	1.595	0.216	-0.040 ± 0.008	0.031
A3530	0.054	563.0	43.94	0	1.310	0.111	-0.040 ± 0.011	0.029
A3532	0.056	621.0	44.45	0	1.250	0.162	-0.038 ± 0.008	0.033
A3556	0.048	558.0	43.97	–	0.160	0.132	-0.037 ± 0.013	0.033
A3558	0.048	915.0	44.80	0	1.575	0.225	-0.040 ± 0.006	0.034
A3560	0.049	710.0	44.12	–	2.255	0.183	-0.034 ± 0.008	0.032
A3667	0.053	993.0	44.94	3	0.950	0.143	-0.048 ± 0.007	0.068
A3716	0.045	833.0	44.00	1	0.125	0.236	-0.049 ± 0.007	0.062
A3809	0.063	563.0	44.35	–	1.170	0.045	-0.065 ± 0.010	0.060
A3880	0.057	763.0	44.27	0	0.540	0.085	-0.043 ± 0.009	0.063
A4059	0.048	715.0	44.49	–	1.125	0.189	-0.040 ± 0.011	0.059
IIZW108	0.048	513.0	44.34	1	0.905	0.031	-0.044 ± 0.010	0.025
MKW3s	0.044	539.0	44.43	1	0.855	0.109	-0.040 ± 0.012	0.030
RX0058	0.048	637.0	43.64	1	0.220	0.097	-0.047 ± 0.013	0.030
RX1022	0.055	577.0	43.54	–	0.135	0.137	-0.075 ± 0.013	0.071
RX1740	0.044	582.0	43.70	3	0.825	0.117	-0.035 ± 0.017	0.031
Z2844	0.050	536.0	43.76	2	0.865	0.038	-0.044 ± 0.018	0.035
Z8338	0.049	712.0	43.90	2	0.710	0.142	-0.051 ± 0.012	0.048
Z8852	0.041	765.0	43.97	2	0.485	0.158	-0.041 ± 0.010	0.032

(2007); Stott et al. (2007); Gilbank et al. (2008); Lu et al. (2009); Rudnick et al. (2009); Stott et al. (2009); Capozzi et al. (2010) and Andreon (2008); Crawford et al. (2009) for opposite conclusions). This is generally interpreted as evidence for a large number of relatively faint galaxies having moved to the RS only recently, most probably due to the quenching of the star formation caused by the high-density environment. The luminous-to-faint ratio has been found to evolve in the field too, but to be lower in clusters than in the field at all redshifts out to $z = 1$, implying that the faint end of the red sequence was established first in clusters (Gilbank & Balogh 2008).

We wish to study how the luminous-to-faint RS ratio changes from cluster to cluster and depends on cluster properties at low redshift. To define the two galaxy populations we corrected our absolute magnitudes for passive evolution: we consider all galaxies brighter than $M_V = -20 - \text{lum}_{\text{corr}}$ to be *luminous*, and all galaxies fainter than this magnitude and brighter than $M_V = -18.2 - \text{lum}_{\text{corr}}$ to be *faint*, where lum_{corr} is the passive evolution correction with respect to $z = 0$. We recall here that these are the same absolute V magnitude limits adopted by De Lucia et al. (2007) and most other works at high redshift, but that high- z studies usually consider the (U-V) rest-frame color, therefore a direct comparison cannot be performed.

Our large sample of local clusters show a large scatter in the luminous-to-faint ratio. In the top panels of Fig.4 and Fig.5 we plot the luminous-to-faint ratio as a function of cluster velocity dispersion, X-ray luminosity, number of substructures, BCG prevalence value and concentration of ellipticals.

As was the case for the RS parameters, no correlation between the luminous-to-faint ratio and the cluster properties is found. This agrees with recent results from Capozzi et al. (2010) who found no relationship between luminous-to-faint ratio and cluster X-ray luminosity at low redshift, and with Rudnick et al. (2009) who failed to detect a dependence of the red galaxy luminosity function on cluster velocity dispersion in the SDSS.

Such lack of a correlation suggests that the downsizing trend in star formation (the different distribution of times at which galaxies turn red and reach the RS depending on their luminosity) does not depend in a simple way from global cluster properties such as the cluster mass, or level of substructure. However, the large scatter of luminous-to-faint values in our sample shows that there is a great diversity in the way the RS is populated as a function of galaxy magnitude. Most likely, this indicates widely different quenching histories in faint galaxies from cluster to cluster, even for clusters of the same mass at $z = 0$.

The blue fraction is defined as the ratio between the number of blue galaxies and the total number of galaxies in the cluster, for $M_V < -18.2$. In the last decade the blue fraction has been observed to have a large scatter of values at any given redshift, and to depend on several obvious parameters such as the magnitude limit used and the cluster-centric distance. However, contrasting conclusions have been reached as to whether it depends on cluster properties such as concentration, richness and presence of substructure (Butcher & Oemler 1984; Wang & Ulmer 1997; Smail et al. 1998; Metevier et al. 2000; Ellingson et al. 2001; Margoniner et al. 2001; Pimblet et al. 2002; Fairley et al. 2002; Balogh et al. 2004; De Propriis et al. 2004; Barkhouse et al. 2009). All these findings together imply that environmental effects may compete with, and possibly mimic, evolutionary trends. Thus, it is of paramount importance to try to disentangle the cluster-to-cluster variance and the dependence on cluster properties in order to properly understand and interpret the studies of high- z clusters and to investigate how the current galaxy populations in clusters came to be.

Figs.4 (bottom panels) shows that in WINGS there is no dependence of the blue fraction on either cluster velocity dispersion or total X-ray luminosity, as found previously in the local Universe and at higher redshifts (Fairley et al. 2002; De Propriis et al. 2004; Goto 2005), and in agreement with a flat median star-forming (emission-line) fraction for clusters with $\sigma > 500 \text{ km s}^{-1}$ in the local Universe (Poggianti et al. 2006; Popesso et al. 2007). Furthermore, we find no trend with the number of substructures, the BCG prevalence value and the concentration of elliptical galaxies (Fig.5). A quite large scatter in the blue fraction is observed fixing any of these parameters, though most clusters have a blue fraction below 20%, with a median of 0.16 ± 0.03 .

Poggianti et al. (2006) proposed a scenario in which the population of passive galaxies (those devoid of ongoing star formation at the time they are observed) consists of two different components: primordial passive galaxies (the most massive, mostly ellipticals), whose stars all formed at $z > 2 - 3$, and quenched galaxies (on average less massive, mostly S0s), whose star formation has been truncated due to the dense environment at later times. Comparing with simulations, they found that at $z = 0$ the observed fraction of passive galaxies in clusters resembles the fraction (in mass and in number of galaxies) that has resided in clusters ($M_{\text{sys}} > 10^{14} M_{\odot}$) during at least the last 3 Gyr.

In this picture, the median fraction of star-forming galaxies, and the median blue fraction we observe, do not correlate with the cluster σ or L_X . This is because in clusters more massive than 500 km s^{-1} at $z = 0$, the median fraction of galaxies that have spent enough time in a massive environment to have their star formation quenched by some (unidentified) environmental mechanism does not vary systematically with cluster mass. This may be a viable explanation also for the lack of correlation between the luminous-to-faint ratio and the global cluster properties, as the blue galaxies and the faint red galaxies together form the overall faint cluster population subject to quenching.

4.3. Morphological fractions and red spirals

When studying the CMD and, more generally, the evolution of galaxy clusters, it is important to evaluate the fractions of the different morphological types residing on the red sequence. Indeed, apart from the well known presence of red Es in galaxy clusters, it is not completely clear if there is some correlation between the frequency of red S0s and late-type galaxies and the global properties of the clusters. The presence of S0s and late-type galaxies on the RS is often ascribed to the capacity of the hostile cluster environment to quench star formation or even strip and/or induce a fading of the disk of galaxies of the later types.

It is apparent from Fig.6 that there is no dependence of the RS morphological fractions on either X-ray luminosity and cluster velocity dispersion. Similarly, no correlations were found with the number of substructures, the BCG prevalence value and the concentration of ellipticals (plot not shown). In the scenario of a double channel for passive galaxies discussed above, this is expected given that the median fractions of both primordial (ellipticals) and quenched galaxies (S0s) are flat with the cluster velocity dispersion (see Fig. 16 in Poggianti et al. (2006)).

The median morphological fractions of galaxies on the RS are 0.35 ± 0.05 for ellipticals, 0.46 ± 0.04 for S0s, 0.17 ± 0.04 for early spirals (Sa to Sbc , $0 < Ttype \leq 4$) and 0.02 ± 0.02 for later type spirals ($4 < T \leq 8$).

It is interesting to compare these values with those found by Sánchez-Blázquez et al. (2009) in clusters at $z = 0.4 - 0.8$, which were obtained adopting similar cluster radial limits and galaxy

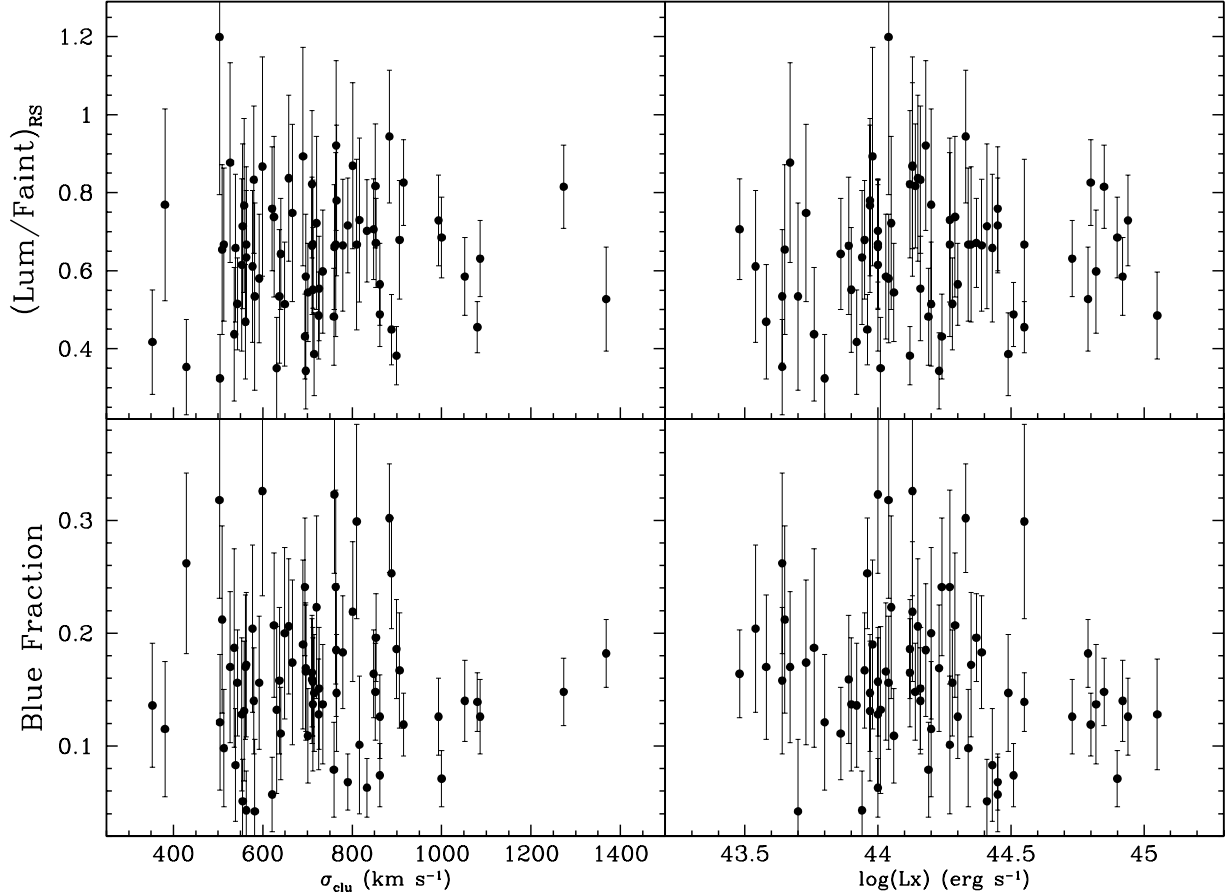


Fig. 4. Luminous-to-faint ratio (top panels) and blue fraction (bottom panels) vs. cluster velocity dispersion and total X-ray luminosity in WINGS clusters. Errorbars are the mean error on the 100 Montecarlo realizations.

magnitude (passively evolved) limits to our study. These authors found an *increase* in the late-type fraction on the red sequence, from 25% at $z = 0.75$ to 44% at $z = 0.45$, due to the fact that the red-sequence becomes more populated at later times with disc galaxies whose star formation has been quenched. Interestingly, however, the same authors predict a subsequent *decrease* of the red late-type fraction from $z = 0.45$ to $z = 0$, due to the combination of the strong morphological evolution from spirals to S0s and the mild variation in the RS luminous-to-faint ratio observed in this redshift interval.

Indeed, our $\sim 20\%$ fraction of late-type galaxies on the RS is much lower than the value observed at $z = 0.45$, and is consistent with a scenario in which over the interval $z = 1 - 0.4$ the RS accretes spirals that have stopped forming stars, a quite large fraction of which are transformed into S0s at $z < 0.4$ (Desai et al. 2007, Dressler et al. 1997, Fasano et al. 2000, Postman et al. 2005).

4.4. Elliptical to S0 ratios and cluster evolution

Regarding the formation history of galaxy clusters, one may expect that clusters with a large presence of red spirals may also have a higher fraction of S0s compared to Es on the RS. In other words, clusters with a larger number of passive late-type galaxies could have transformed a larger number of them into S0s.

Figure 7 shows the relation between the RS late-type fraction and the RS ratio of Es to S0s. Clusters with a larger fraction of red spirals tend to have a population of early-type galaxies on the RS dominated by S0 morphologies. According to the Spearman test the E/S0 number ratio on the RS is anticorrelated with the late type fraction on the RS with a 95% probability.

5. The main driver: the local density

In the previous sections we have shown that the RS parameters, luminous-to-faint ratio, blue fraction and morphological fractions on the RS do not depend on cluster global properties such as velocity dispersion or X-ray luminosity, nor on elliptical galaxy concentration, BCG prevalence or number of substructures.

In Figs. 8 and 9 we show that all the galaxy properties considered do, however, vary with the local galaxy density. Most noticeably, higher density regions have a tighter RS (lower RS scatter), and a lower fraction of blue galaxies. The RS generally becomes steeper (RS slope increases) with local density, except for a high value in the lowest density bin. We note that a dependence of the location of the CM relation and of the blue fraction on local density has been found before in the Shapley supercluster at $z=0.05$ by Haines et al. (2006).

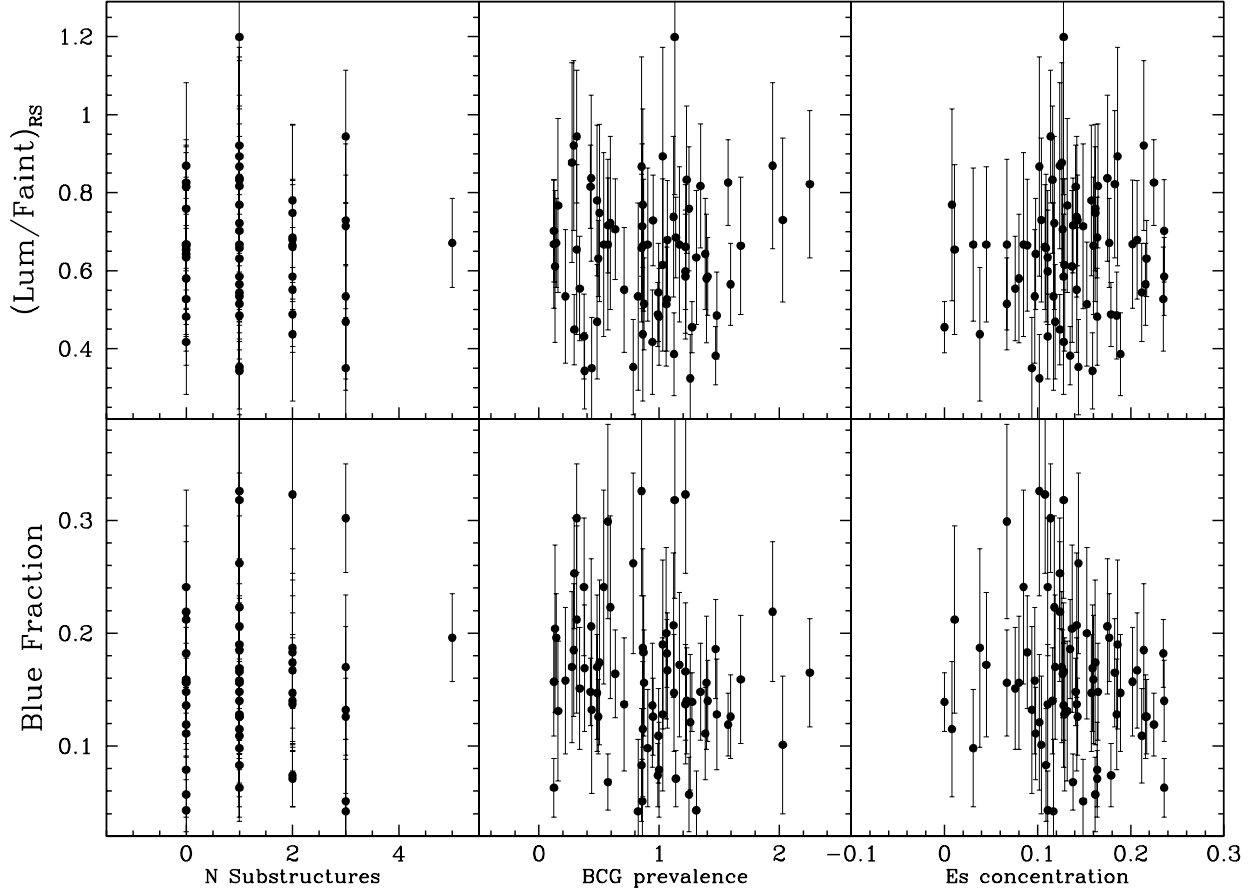


Fig. 5. Luminous-to-faint ratio (top panels) and blue fraction (bottom panels) vs. number of substructures, BCG prevalence value and concentration of elliptical galaxies in WINGS clusters. Errorbars are the mean error on the 100 Montecarlo realizations.

The high RS slope in the lowest density bin is accompanied by slightly higher values of the fraction of ellipticals and of the E/S0 number ratio compared to denser regions (Fig.9). It is hard to assess the significance of these single points, and wider images will be needed to sample lower density outer regions of clusters.

Interestingly, the RS luminous-to-faint ratio increases monotonically with local density (Fig. 8), implying that the relative proportion of luminous red galaxies and faint red galaxies is higher in denser regions. This is the first time such a trend is observed. At high- z , the opposite trend has been found, consistent with the fact that the build-up of the CMR is delayed in lower density environments (Tanaka et al. 2005; Tanaka et al. 2007). The increase of the luminous-to-faint ratio with density in WINGS clusters seems to reflect, instead, the fact that WINGS higher density regions host proportionally more high-mass than low-mass galaxies (regardless of color) than lower density regions, as shown in Vulcani et al. (2011).

Finally, higher density regions have a lower fraction of spirals on the RS than lower density regions (Fig.9): the RS in the highest density regions includes only a few spirals ($\sim 10\%$), while the RS in low density regions is composed by up to 30% of spirals. The relative proportion of ellipticals and S0s does not change with local density, except for the highest density regions where ellipticals dominate.

It is important to stress that the correlations between RS properties and local density shown in Fig.8 are *not* driven by differences between the RS properties of the different morphological types in combination with the morphology-density relation. In particular, we wished to test whether a larger fraction of spirals at low densities might induce the trends observed. We found that none of the conclusions from Fig.8 change if we only include ellipticals, only S0s, or only ellipticals+S0s.

6. Discussion and conclusions

In this work we have analyzed the properties of the (B-V) versus V color-magnitude red sequence of 72 X-ray selected clusters at $z = 0.04 - 0.07$ from the WINGS survey.

We have searched for correlations between the characteristics of the RS and the properties of both the global and local environment, finding the following main results:

- The location and parameters of the RS, as well as the magnitude and morphological distributions of its galaxies, do not depend on global cluster properties. Specifically:
 - neither the slope nor the scatter of the RS, nor
 - the number ratio of luminous-to-faint galaxies on the RS, nor
 - the fraction of blue galaxies, nor

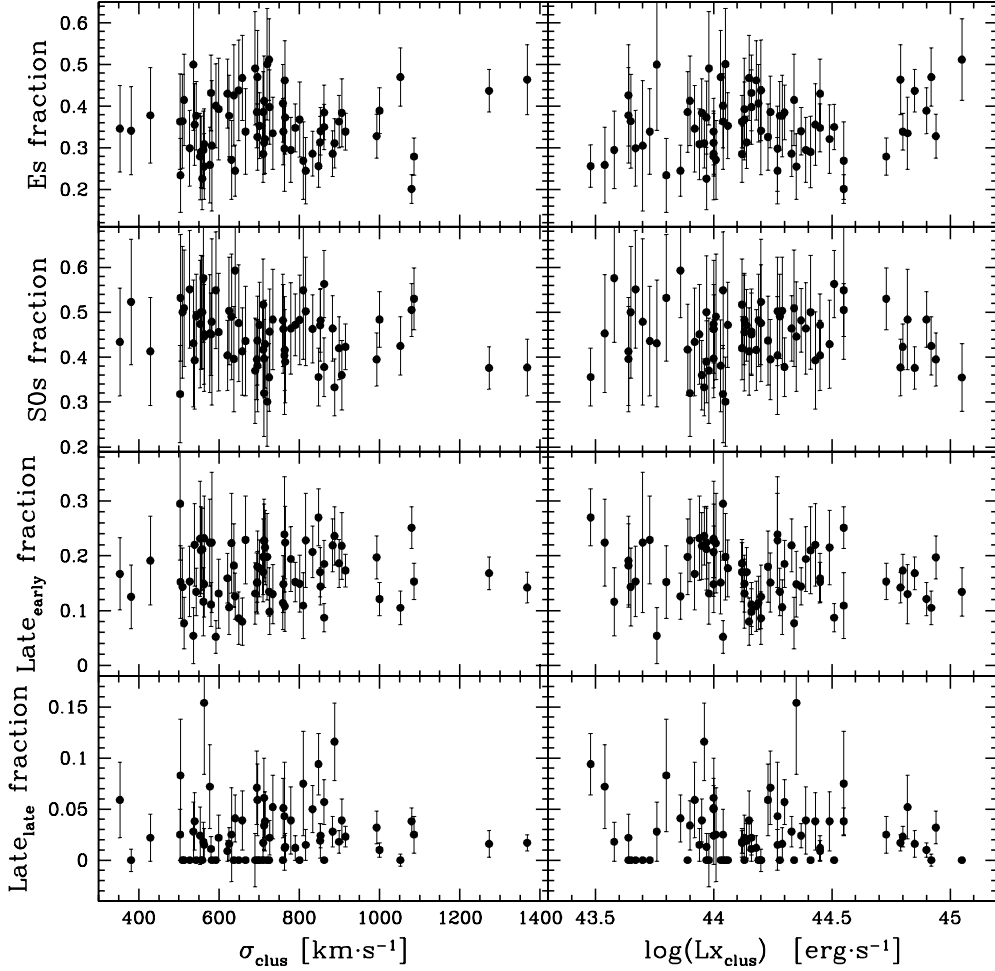


Fig. 6. Morphological fractions on the RS vs. central velocity dispersion and total X-ray luminosity of the WINGS clusters. Errorbars are the mean error on the 100 Monte Carlo realizations. “Early” late-type galaxies are Sa’s and Sb’s, while “Late” late-type galaxies are Sc’s and later.

- the morphological mix on the RS, that is, the fraction of galaxies on the RS that are ellipticals, S0s and spirals,

none of the above vary systematically with cluster velocity dispersion nor X-ray luminosity (hence with cluster mass), nor with the number of substructures, BCG magnitude separation from the next brightest galaxies nor spatial concentration of elliptical galaxies.

- We find a weak tendency for clusters whose RS is “rich” in S0 galaxies (compared to the population of ellipticals) to be also “rich” in red spirals. The populations of S0 and spirals on the RS are coupled at some level.
- The strongest correlations we find are between the RS and the local galaxy density. The scatter and, possibly, the slope of the RS vary with local density, as do the luminous-to-faint ratio, blue galaxy fraction and morphological mix of galaxies on the RS. The latter means that, remarkably, a clear morphology-density relation, especially for spirals, is visible even restricting the analysis to galaxies on the red sequence.

However, the correlations between RS properties and local density are not due to the morphology-density relation (i.e. a higher fraction of spirals at lower densities), as all the trends

- in Fig.8 persist even when restricting the analysis to only ellipticals, only S0s, or only early-type galaxies.

These trends suggest that galaxies in higher density regions within clusters became passive and evolved morphologically towards earlier types at earlier epochs than galaxies in lower density regions that are today *within the same clusters*, as witnessed by the lower RS scatter, lower blue fraction, and lower spiral fraction on the RS at higher densities.

Local density thus appears to be the main factor governing the evolutionary pace of galaxies in these clusters. If this is the case, the lack of a trend of the RS characteristics with the cluster mass is not surprising, given that the distribution of local galaxy densities does not depend on cluster mass (Poggianti et al. 2010).

In the same way as the morphological mix of galaxies (of all colors) depends on local density (Dressler 1980) and not on cluster mass (Poggianti et al. 2009) in the local Universe, this work highlights the prominent effect of the local density as opposed to the mass of the galaxy host structure in setting the passivization epoch of galaxies and their arrival on the RS, and the subsequent morphological transformation to S0s.

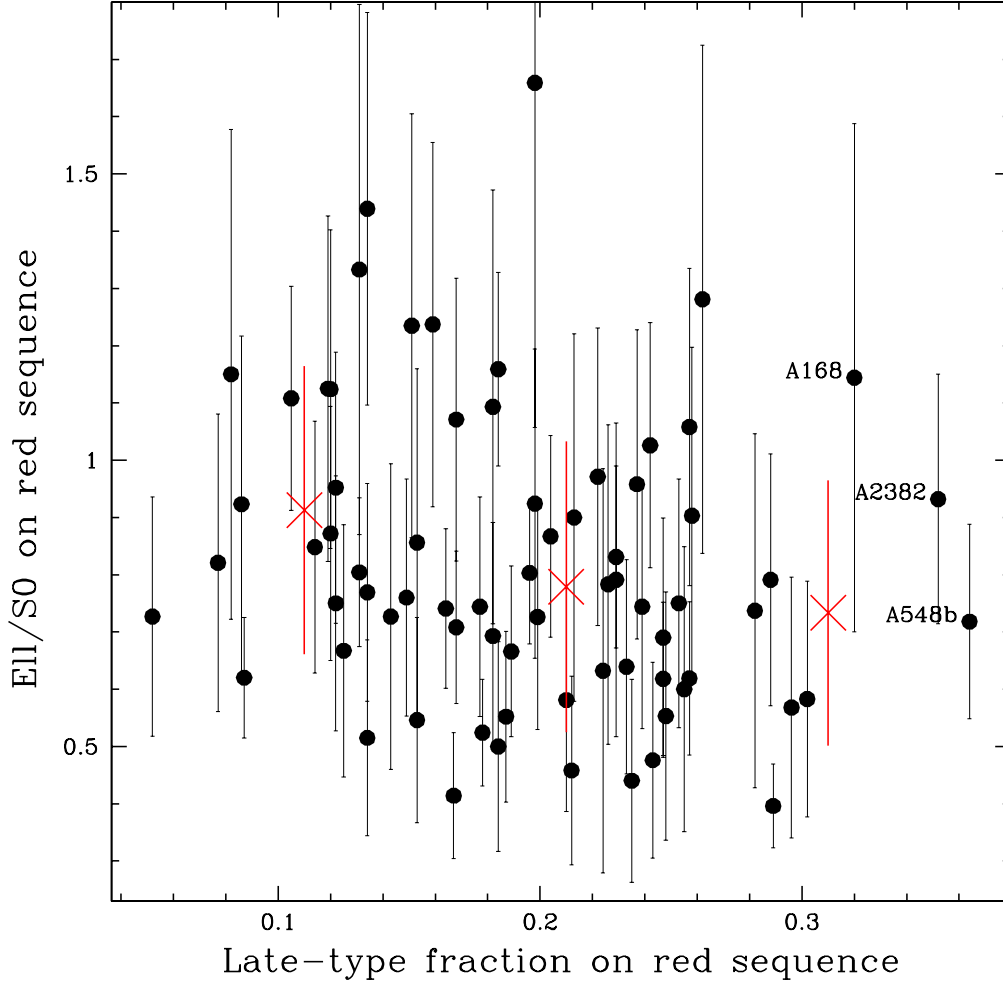


Fig. 7. Ellipticals over S0s number ratio on the RS vs. late-type fraction on the RS. Errorbars are the mean error on the 100 Montecarlo realizations. Red crosses and corresponding errorbars represent the mean E/S0 values and their sigma in three bins of late-type fraction.

The dependence of the RS properties on local density can originate from several mechanisms, and at different cosmological epochs. Since the present local density is expected to correlate with the initial density in the primordial phases, the star formation process may be accelerated in dense regions from the start, yielding shorter formation times. Physical processes acting at later times, among those commonly referred to as environmental mechanisms, can accelerate and/or quench star formation more efficiently in denser regions. Among these, there are gravitational interactions between galaxies, before or after the accretion of galaxies onto clusters, and gas removal mechanisms. While a detailed modeling of such processes is beyond the scope of this paper, the combination of the lack of trends with cluster mass and of the observed correlations with local density represent a solid observational constraint for future studies.

References

- Abraham, R. G., van den Bergh, S., & Nair, P. 2003, *ApJ*, 588, 218
 Andreon, S. 2008, *MNRAS*, 386, 1045
 Balogh, M. L., Baldry, I. K., Nichol, R., Miller, C., Bower, R., & Glazebrook, K. 2004, *ApJ*, 615, L101
 Balogh, M. L., et al. 2009, *MNRAS*, 398, 754
 Barkhouse, W. A., Yee, H. K. C., & López-Cruz, O. 2009, *ApJ*, 703, 2024
 Bell, E. F., et al. 2004, *ApJ*, 608, 752
 Bell, E. F., Zheng, X. Z., Papovich, C., Borch, A., Wolf, C., & Meisenheimer, K. 2007, *ApJ*, 663, 834
 Bekki, K. 2009, *MNRAS*, 399, 2221
 Berta, S., Rubele, S., Franceschini, A., et al. 2006, *A&A*, 451, 881
 Bower, R. G., Lucey, J. R., & Ellis, R. S. 1992, *MNRAS*, 254, 589
 Bower, R. G., Benson, A. J., Malbon, R., Helly, J. C., Frenk, C. S., Baugh, C. M., Cole, S., & Lacey, C. G. 2006, *MNRAS*, 370, 645
 Butcher, H., & Oemler, A., Jr. 1984, *ApJ*, 285, 426
 Capozzi, D., Collins, C. A., & Stott, J. P. 2010, *MNRAS*, 403, 1274
 Cava, A., Bettoni, D., Poggianti, B. M., et al. 2009, *A&A*, 495, 707
 Cheng, J. Y., Faber, S. M., Simard, L., Graves, G. J., Lopez, E. D., Yan, R., & Cooper, M. C. 2011, *MNRAS*, 412, 727
 Conselice, C. J. 2003, *ApJS*, 147, 1
 Conselice, C. J., Bershady, M. A., & Jangren, A. 2000, *ApJ*, 529, 886
 Cowie, L. L., Songaila, A., Hu, E. M., & Cohen, J. G. 1996, *AJ*, 112, 839
 Crawford, S. M., Bershady, M. A., & Hoessel, J. G. 2009, *ApJ*, 690, 1158
 Croton, D. J., et al. 2006, *MNRAS*, 365, 11
 Dariush, A. A., Raychaudhury, S., Ponman, T. J., Khosroshahi, H. G., Benson, A. J., Bower, R. G., & Pearce, F. 2010, *MNRAS*, 405, 1873
 De Lucia, G., et al. 2004, *ApJ*, 610, L77
 De Lucia, G., Poggianti, B. M., Aragón-Salamanca, A., et al. 2007, *MNRAS*, 374, 809
 De Propriis, R., et al. 2004, *MNRAS*, 351, 125
 Desai, V., et al., 2007, *ApJ*, 660, 1151

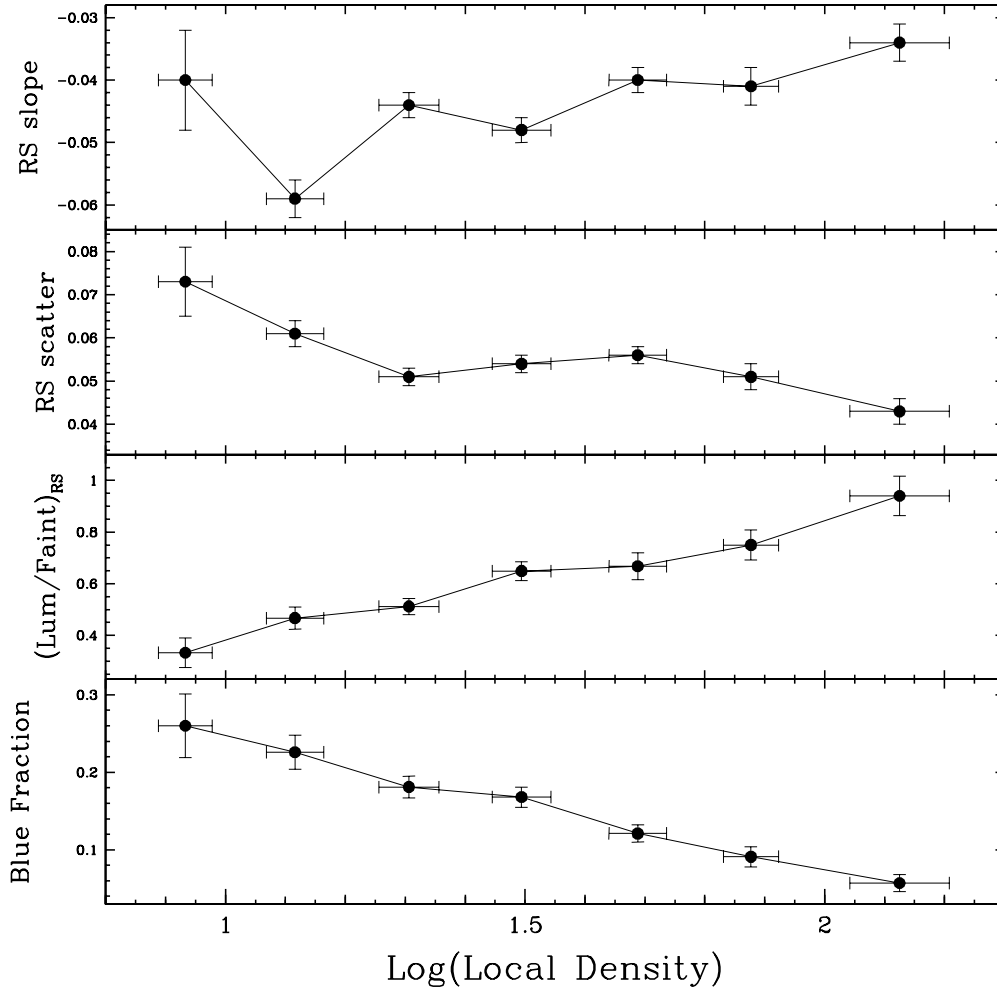


Fig. 8. RS slope and scatter, luminous-to-faint ratio and blue fraction vs. galaxy local density.

- de Vaucouleurs, G. 1961, *ApJS*, 5, 233
Dressler, A. 1980, *ApJ*, 236, 351
Dressler, A., Oemler, A., Couch, W.J., Smail, I., Ellis, R.S., Barger, A., Butcher, H., Poggianti, B.M., Sharples, R.M., 1997, *ApJ*, 490, 577
Ebeling, H., Edge, A. C., Allen, S. W., et al. 2000, *MNRAS*, 318, 333
Ebeling, H., Edge, A. C., Bohringer, H., et al. 1998, *MNRAS*, 301, 881
Ebeling, H., Voges, W., Bohringer, H., et al. 1996, *MNRAS*, 281, 799
Ellingson, E., Lin, H., Yee, H. K. C., & Carlberg, R. G. 2001, *ApJ*, 547, 609
Ellis, R. S., Smail, I., Dressler, A., Couch, W. J., Oemler, A., Jr., Butcher, H., & Sharples, R. M. 1997, *ApJ*, 483, 582
Faber, S. M., et al. 2007, *ApJ*, 665, 265
Fairley, B. W., Jones, L. R., Wake, D. A., Collins, C. A., Burke, D. J., Nichol, R. C., & Romer, A. K. 2002, *MNRAS*, 330, 755
Fasano, G., Poggianti, B. M., Couch, W. J., et al. 2000, *ApJ*, 542, 673
Fasano, G., Bettoni, D., Ascaso, B., et al. 2010, *MNRAS*, 404, 1490
Fasano, G., Vanzella, E., Dressler, A., et al. 2011, submitted
Fasano, G., Marmo, C., Varela, J., et al. 2006, *A&A*, 445, 805
Font, A. S., et al. 2008, *MNRAS*, 389, 1619
Gilbank, D. G., Yee, H. K. C., Ellingson, E., Gladders, M. D., Loh, Y.-S., Barrientos, L. F., & Barkhouse, W. A. 2008, *ApJ*, 673, 742
Gilbank, D. G., & Balogh, M. L. 2008, *MNRAS*, 385, L116
Gilbank, D. G., Gladders, M. D., Yee, H. K. C., & Hsieh, B. C. 2011, *AJ*, 141, 94
Gladders, M. D., & Yee, H. K. C. 2005, *ApJS*, 157, 1
Goto, T. 2005, *MNRAS*, 356, L6
Gunn, J. E., & Gott, J. R., III 1972, *ApJ*, 176, 1
Guo, Q., et al. 2011, *MNRAS*, 413, 101
Haines, C.P., Merluzzi, P., Mercurio, A., Gargiulo, A., Krusanova, N., Busarello, G., la Barbera, F., Capaccioli, M., 2006, *MNRAS*, 371, 55
Kauffmann, G., et al. 2003, *MNRAS*, 341, 54
Kimm, T., et al. 2009, *MNRAS*, 394, 1131
Kodama, T., Arimoto, N., Barger, A. J., & Arag' on-Salamanca, A. 1998, *A&A*, 334, 99
Kodama, T. & Bower, R. G. 2001, *MNRAS*, 321, 18
Lidman, C., et al. 2008, *A&A*, 489, 981
Loh, Y.-S., Ellingson, E., Yee, H. K. C., Gilbank, D. G., Gladders, M. D., & Barrientos, L. F. 2008, *ApJ*, 680, 214
Lotz, J. M., Primack, J., & Madau, P. 2004, *AJ*, 128, 163
Lu, T., Gilbank, D. G., Balogh, M. L., & Bognat, A. 2009, *MNRAS*, 399, 1858
Margoniner, V. E., de Carvalho, R. R., Gal, R. R., & Djorgovski, S. G. 2001, *ApJ*, 548, L143
McCarthy, I. G., et al. 2010, *MNRAS*, 406, 822
Mei, S., et al. 2009, *ApJ*, 690, 42
Metevier, A. J., Romer, A. K., & Ulmer, M. P. 2000, *AJ*, 119, 1090
Moore, B., Lake, G., & Katz, N. 1998, *ApJ*, 495, 139
Muzzin, A., et al. 2009, *ApJ*, 698, 1934
Omizzolo, A., Fritz, J., Poggianti, B. M., et al. 2011, in preparation
Peng, Y., Lilly, S.J., Kovac, K., et al., 2010, *ApJ*, 721, 193
Pimblett, K. A., Smail, I., Kodama, T., et al. 2002, *MNRAS*, 331, 333
Poggianti, B. M. 1997, *A&AS*, 122, 399
Poggianti, B. M., et al. 2006, *ApJ*, 642, 188
Poggianti, B. M., Fasano, G., Bettoni, D., et al. 2009, *ApJ*, 697, L137
Poggianti, B. M., De Lucia, G., Varela, J., Aragon-Salamanca, A., Finn, R., Desai, V., von der Linden, A., & White, S. D. M. 2010, *MNRAS*, 405, 995
Popesso, P., Biviano, A., Romaniello, M., & Böhringer, H. 2007, *A&A*, 461, 411
Postman, M. et al., 2005, *ApJ*, 623, 721
Ramella, M., Biviano, A., Pisani, A., et al. 2007, *A&A*, 470, 39
Rudnick, G., et al. 2009, *ApJ*, 700, 1559

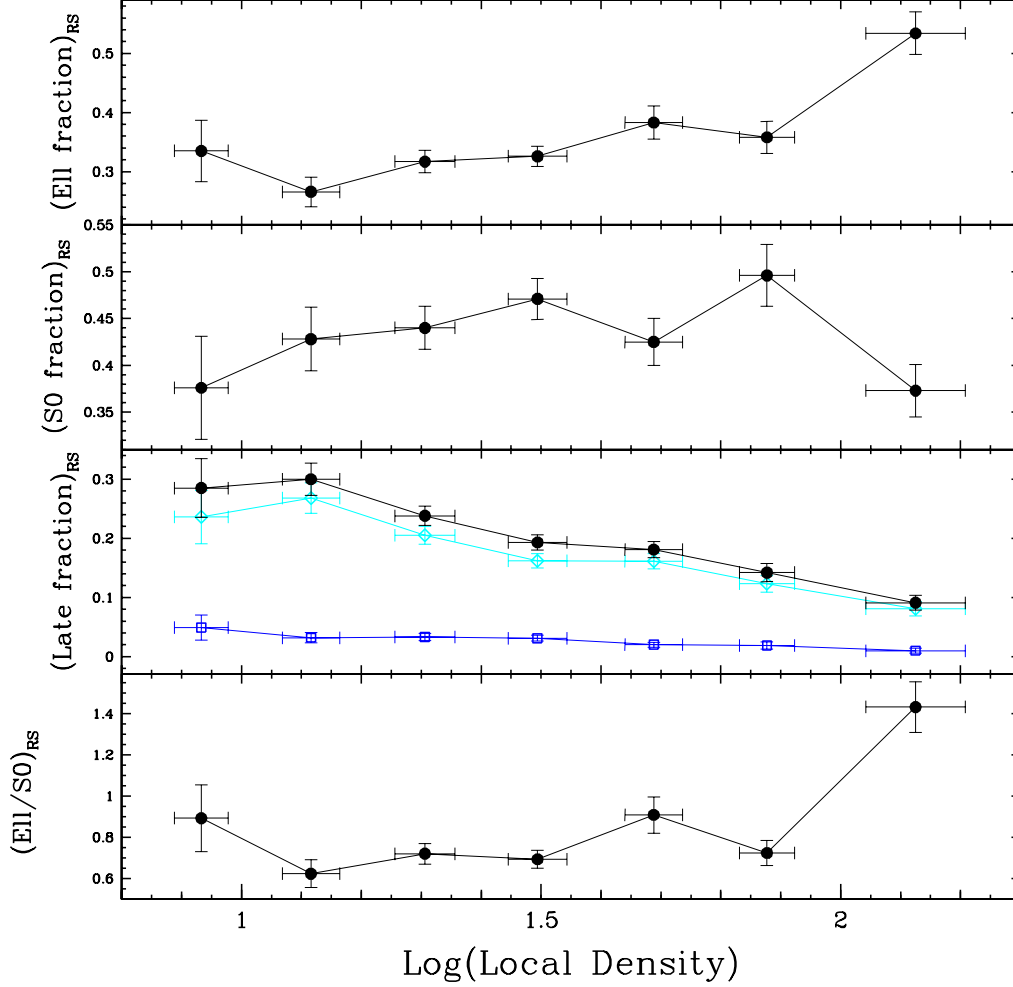


Fig. 9. Morphological fractions on the RS vs galaxy local density. From top to bottom: ellipticals, S0s, later-types (early-spirals and late spirals, cyan diamonds and blue squares, respectively) and E/S0 ratio.

Sánchez-Blázquez, P., et al. 2009, *A&A*, 499, 47
 Smail, I., Edge, A. C., Ellis, R. S., & Blandford, R. D. 1998, *MNRAS*, 293, 124
 Stott, J. P., Smail, I., Edge, A. C., Ebeling, H., Smith, G. P., Kneib, J.-P., & Pimblett, K. A. 2007, *ApJ*, 661, 95
 Stott, J. P., Pimblett, K. A., Edge, A. C., Smith, G. P., & Wardlow, J. L. 2009, *MNRAS*, 394, 2098
 Strateva, I., et al. 2001, *AJ*, 122, 1861
 Strazzullo, V., et al. 2010, *A&A*, 524, A17
 Tanaka, M., Kodama, T., Arimoto, N., et al. 2005, *MNRAS*, 362, 268
 Tanaka, M., Kodama, T., Kajisawa, M., Bower, R., Demarco, R., Finoguenov, A., Lidman, C., & Rosati, P. 2007, *MNRAS*, 377, 1206
 Valentinuzzi, T., Woods, D., Fasano, G., et al. 2009, *A&A*, 501, 851
 van den Bosch, F. C., Aquino, D., Yang, X., Mo, H. J., Pasquali, A., McIntosh, D. H., Weinmann, S. M., & Kang, X. 2008, *MNRAS*, 387, 79
 Varela, J., D’Onofrio, M., Marmo, C., et al. 2009, *A&A*, 497, 667
 Visvanathan, N., & Sandage, A. 1977, *ApJ*, 216, 214
 Wang, Q. D., & Ulmer, M. P. 1997, *MNRAS*, 292, 920
 Wilson, G., et al. 2009, *ApJ*, 698, 1943

of Technology, under contract with the National Aeronautics and Space Administration.

IRAF (Image Reduction and Analysis Facility) is written and supported by the IRAF programming group at the National Optical Astronomy Observatories (NOAO) in Tucson, Arizona. NOAO is operated by the Association of Universities for Research in Astronomy (AURA), Inc. under cooperative agreement with the National Science Foundation.

Acknowledgements. We thank the anonymous referee for her/his comments that led to improvements of this paper, and Diego Capozzi for useful discussions and comments.

T. Valentinuzzi acknowledges a post-doc fellowship from the Ministero dell’Istruzione, dell’Università e della Ricerca (Italy). BV and BMP acknowledge financial support from ASI contract I/016/07/0.

This research has made use of the NASA/IPAC Extragalactic Database (NED) which is operated by the Jet Propulsion Laboratory, California Institute